Available online at www.sciencedirect.com
SCIENCE DIRECT®
Atmospheric Environment 39 (2005) 7351–7361
ATMOSPHERIC ENVIRONMENT
www.elsevier.com/locate/atmosenv

A scheme for drag partition over rough surfaces

Yaping Shao*, Yan Yang

Department of Physics and Materials Science, City University of Hong Kong, Hong Kong SAR, China

Received 21 March 2005; received in revised form 7 August 2005; accepted 2 September 2005

Abstract

We present a drag partition scheme for surfaces of various roughness densities. The total drag is partitioned into three components: a pressure drag, a skin drag due to momentum transfer to the surfaces of roughness elements and a surface drag due to momentum transfer to the ground surface. We introduce an effective frontal area index to characterize the mutual sheltering effect of roughness elements on drag partition and propose a method for the calculation of the drag components. The drag partition scheme is then applied to the calculation of bulk quantities such as roughness length and zero-plane displacement height. The results are compared with wind-tunnel measurements. Roughness length is found to increase with frontal area index λ to a maximum at about $\lambda = 0.2$, and then decreases with λ. This finding is in agreement with observations. The drag partition scheme has applications to studying scalar exchange in boundary layers over rough surfaces, such as urban boundary layers.

Keywords: Drag partition; Effective frontal area index; Roughness length; Rough surface; Turbulence

1. Introduction

The main concern of this study is drag and drag partition in atmospheric boundary layers over rough surfaces. In previous studies (e.g. Schlichting, 1936; Wooding et al., 1973; Arya, 1975; Raupach, 1992), the total drag on a rough surface is partitioned into a pressure drag τ_{tp} on the roughness elements and a skin drag τ_{ts} on the underlying surface:

$$\tau = \tau_{tp} + \tau_{ts}. \tag{1}$$

A quantity often used for characterizing a rough surface is frontal area index (or roughness density) λ

$$\lambda = \frac{Nbh}{S}, \tag{2}$$

where N is the number of roughness elements, b and h are the typical width and height of the roughness elements and S is the surface area.

Raupach (1992) developed a drag partition scheme by introducing the concepts of effective sheltering and random superposition of effective sheltering areas and volumes. The main result of that study is

$$\frac{\tau_{ts}}{\tau} = \frac{1}{1+\beta\lambda}, \quad \frac{\tau_{tp}}{\tau} = \frac{\beta\lambda}{1+\beta\lambda}, \tag{3}$$

where $\beta = C_R/C_S$ is the ratio of the drag coefficient for isolated roughness element (C_R) to that for bare surface (C_S). Raupach et al. (1993) applied the scheme to determining the threshold friction velocity for wind erosion, u_{*t} and found that the ratio $R_t = u_{*tS}/u_{*tR}$, with u_{*tS} being the threshold friction velocity for the smooth surface and u_{*tR} for the

*Corresponding author. Tel.: +852 2788 9978; fax: +852 2788 7830.
E-mail address: apyshao@cityu.edu.hk (Y. Shao).

1352-2310/$ - see front matter © 2005 Elsevier Ltd. All rights reserved.
doi:10.1016/j.atmosenv.2005.09.014

Nomenclature

A	effective shelter area, L^2
b	typical width of roughness element, L
C_R	drag coefficient for isolated roughness elements
C_S	drag coefficient for surface
d	zero-plane displacement height, L
d_a	centroid of $(\tau_{tb}+\tau_{ts})$, L
d_{tb}	centroid of τ_{tb}, L
d_{tp}	centroid of τ_{tp}, L
d_{ts}	centroid of τ_{ts}, L
h	typical height of roughness element, L
K	eddy viscosity, $L^2\,T^{-1}$
l	typical length of roughness element, L
N	number of roughness elements
r_{tb}	ratio of skin drag to total drag
r_{tp}	ratio of pressure drag to total drag
r_{ts}	ratio of surface drag to total drag
S	surface area covered by roughness elements, L^2
U_r	flow velocity at reference level, $L\,T^{-1}$
$u(z)$	flow velocity at height z, $L\,T^{-1}$
u_*	friction velocity, $L\,T^{-1}$
u_{*a}	friction velocity related to $(\tau_{tb}+\tau_{ts})$, $L\,T^{-1}$
V	effective shelter volume, L^3
w_c	typical streamwise inter-element distance, L
z	height, L
z_w	height, for $z>z_w$ logarithmic wind profile is valid, L
z_0	aerodynamic roughness length, L
z_{0s}	roughness length of roughness element surface, L
κ	von Karman constant
λ	frontal area index (or roughness density)
λ_a	value of λ at which u_*/U_r is maximum
λ_c	value of λ at which pressure drag starts to decrease
λ_e	effective frontal area index
λ_{max}	maximum frontal area index
ρ	air density, $M\,L^{-3}$
η	plane area index
β	ratio of C_R/C_S
τ	total drag, $C_R M\,L^{-1}\,T^{-2}$
τ_{tb}	skin drag on surface of roughness elements, $M\,L^{-1}\,T^{-2}$
τ_{tp}	pressure drag, $M\,L^{-1}\,T^{-2}$
τ_{ts}	surface drag, $M\,L^{-1}\,T^{-2}$
τ_a	sum of $\tau_{tb}+\tau_{ts}$, $M\,L^{-1}\,T^{-2}$
σ_a	roughness element aspect ratio $(-b/h)$
σ_c	ratio of roughness element height to streamwise inter-element distance

rough surface, can be expressed as

$$R_t=\left[\frac{1}{(1-m\sigma\lambda)(1+m\beta\lambda)}\right]^{1/2}, \tag{4}$$

where σ is the ratio of roughness element basal area to frontal area, and m is an empirical parameter. Eq. (4) has been tested in several experimental studies (e.g. Wolfe and Nickling, 1996) and is generally supported by experimental data although there are uncertainties in the values of β and m. Both β and m appear to depend on the roughness element aspect ratio (Crawley and Nickling, 2003). The value of C_R requires further study, especially for surfaces with porous roughness elements (Gillies et al., 2000).

The validity of Eqs. (3) and (4) is limited to $\lambda\leqslant 0.1$. In practice, we often encounter rough surfaces (e.g. urban surfaces) with much larger roughness densities. For such surfaces, drag partition is made more complicated by the interactions of turbulent wakes and mutual sheltering of roughness elements, and to our knowledge, suitable drag partition schemes have not yet been developed. The understanding of drag and drag partition is important to studying scalar transfer in atmospheric boundary layers over rough surfaces, e.g., air pollution dispersion from urban canyons, dust emission from Aeolian surfaces and energy fluxes from vegetation canopies. There are two specific problems in this regard: (1) the drag partition theory is key to developing parameterization schemes for scalar transfer over rough surfaces; and (2) it allows the estimation of macro-scopic parameters, such as aerodynamic roughness length and zero-plane displacement height. Both problems have been subject to a number of studies (e.g. Bottema, 1996; Macdonald et al., 1998; Harman et al., 2004). In this study, we propose a drag partition scheme which is applicable to a wide range of roughness densities (Section 2). For $\lambda\leqslant 0.1$, our scheme reduces to the Raupach (1992) scheme. The proposed scheme is then applied to estimating roughness length z_0 and zero-plane displacement height d for rough surfaces. The estimated z_0 and d are compared with several

wind-tunnel data sets (e.g. Hall et al., 1996) as well as with the estimates of Macdonald et al. (1998) in Section 3. The conclusions are given in Section 4. The application of the drag partition scheme to studying scalar transfer in urban boundary layers will be described in Yang and Shao (2005).

2. Drag partition scheme

In addition to λ, we introduce a skin area index, η, for characterizing a rough surface,

$$\eta = \frac{Nbl}{S}, \tag{5}$$

where l is the typical length of the roughness elements. For roughness elements such as square blocks (i.e., $b = l$, often used in wind-tunnel experiments), the relationship between λ and η is

$$\eta = \sigma_a \lambda, \tag{6}$$

where $\sigma_a = b/h$ is the roughness element aspect ratio. For cubic blocks, $\sigma_a = 1$ and $\eta = \lambda$.

Eq. (3) suggests that $\tau_{tp}/\tau \longrightarrow 0$ as $\lambda \longrightarrow 0$ and $\tau_{tp}/\tau \longrightarrow 1$ as $\lambda \longrightarrow \infty$. The latter extrapolation is obviously incorrect, as the Raupach (1992) scheme is valid for $\lambda \leqslant 0.1$ or so. To facilitate descriptions, we suppose the roughness elements are square blocks. In this case, the maximum frontal area index is $\lambda_{max} = 1/\sigma_a$. As the amount of roughness elements increases to a level exceeding a critical value, λ_c, the mutual sheltering among the roughness elements would start to dominate and the pressure drag to decrease. As $\lambda \longrightarrow \lambda_{max}$, τ_{tp}/τ should be zero, and τ_{ts}/τ should also be zero, as the ground surface is now fully covered by roughness elements. Hence, the partition of total drag into two components is inadequate for the situation of large λ, instead it should be partitioned into three components

$$\tau = \tau_{tp} + \tau_{ts} + \tau_{tb}, \tag{7}$$

where τ_{tb} is the skin drag due to the momentum transfer to the surfaces of roughness elements.

In deriving the drag partition theory, Raupach (1992) introduced the concept effective shelter area, A, and effective shelter volume, V, and suggested that

$$A = c\frac{\lambda S}{N}\frac{U_r}{u_*},$$
$$V = Ah,$$

where c is a constant of order one and N is the number of roughness elements. Fig. 1a illustrates Raupach's concept of effective sheltering. In case of small λ, the above expressions are adequate as the turbulent wakes are almost isolated. As λ increases, these expressions become less adequate as the interactions among turbulent wakes become more important. In fact, if λ exceeds a critical value, Eq. (18) in Raupach (1992) does not have a solution. The difficulty now is how to quantify the effect of wake interactions on drag partition. In this study, we introduce an effective frontal area index λ_e to represent this effect. We argue that as roughness density increases, individual roughness elements become less effective in generating A and V, i.e., only a fraction of the roughness elements can be seen by the mean flow. Our argument is illustrated in Fig. 1b which shows that in case of wake interference, A is reduced. We can now define

$$A_e = c\frac{\lambda_e S}{N}\frac{U_r}{u_*},$$
$$V_e = A_e h,$$

with λ_e being the effective frontal area index, which can be understood as the fraction of frontal area that generates sheltering.

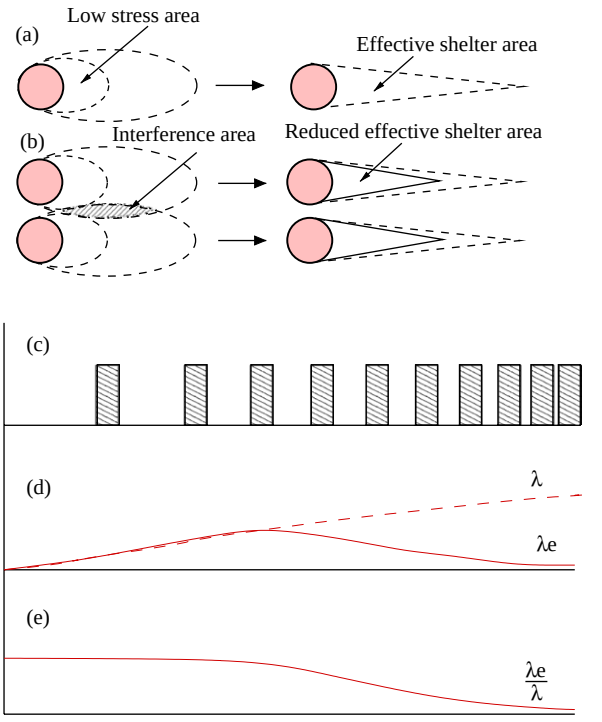

Fig. 1. An illustration of effective frontal area index, λ_e. (a) Effective shelter area; (b) effective shelter area is reduced in case of large roughness density; (c) A surface covered by roughness elements with various separation; (d) the hypothetic behavior of λ and λ_e as the number of roughness elements increases; and (e) the hypothetic ratio of λ_e to λ.

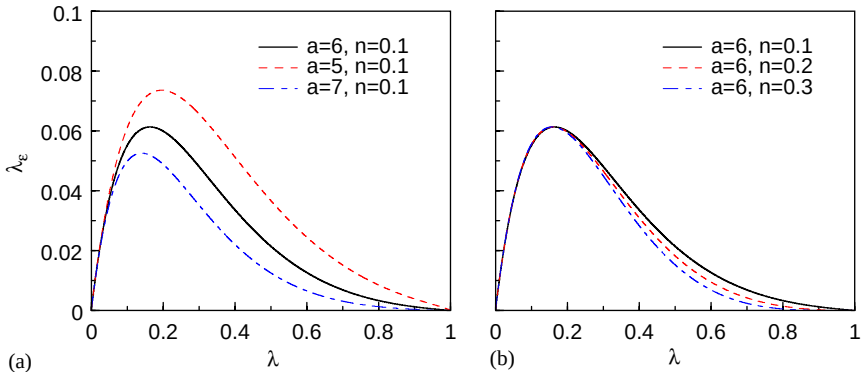

Fig. 2. Dependence of λ_e on λ for different choices of a and n in Eq. (8).

It is not exactly known how λ_e should be calculated. However, the constraints on λ_e are obvious

$$\lambda_e/\lambda = 1 \quad \lambda \to 0,$$
$$\lambda_e/\lambda = 0 \quad \lambda \to \lambda_{max}.$$

Further, measurements show that z_0 reaches a maximum at about $\lambda = 0.2$ (see Bottema (1996) for a summary) which suggests that λ_e should also be a maximum at this value of λ. The following choice of λ_e satisfies these constraints

$$\lambda_e = \frac{\lambda}{(1-\eta)^n} \exp\left[-\frac{a\lambda}{(1-\eta)^n}\right], \tag{8}$$

where n and a are constants that are yet to be estimated. Fig. 2 shows a plot of λ_e against λ for cubic roughness elements for various choices of a and n. For given n (Fig. 2a), a affects both the magnitude of λ_e and the location of the peak value; for given a (Fig. 2b) n mainly affects the decay of λ_e with λ for large λ. We select $a = 6$ and $n = 0.1$ as default choices. The choice of $a = 6$ ensures λ_e reaches the maximum at around $\lambda = 0.2$. Other choices of a and n are used for sensitivity tests.

We now consider the behavior of U_r/u_* with u_* being friction velocity and U_r the representative mean flow velocity of the boundary layer. In some studies, U_r is the mean flow velocity at the level of roughness element height. Raupach (1992) suggested that

$$\frac{U_r}{u_*} = \begin{cases} (C_S + \lambda C_R)^{-1/2} \exp\left(\dfrac{c\lambda}{2}\dfrac{U_r}{u_*}\right) & \lambda \leqslant \lambda_a \\ (C_S + \lambda_a C_R)^{-1/2} \exp\left(\dfrac{c\lambda_a}{2}\dfrac{U_r}{u_*}\right) & \lambda > \lambda_a, \end{cases} \tag{9}$$

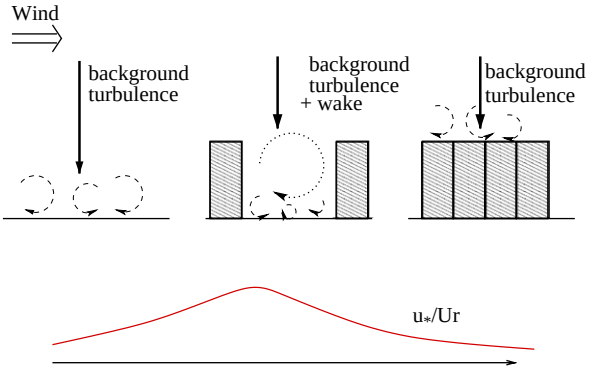

Fig. 3. An illustration of the processes that affect the u_*/U_r dependency on λ.

where λ_a is the value of λ at which u_*/U_r is maximum. Eq. (9) fits well to the data of Raupach et al. (1980) and O'Loughlin (1965). The value of λ_a is about 0.2 and for $\lambda > \lambda_a$, Eq. (9) suggests u_*/U_r is constant.

Again, the behavior of u_*/U_r is not well known for large λ values. Eq. (9) suggests that u_*/U_r is constant for $\lambda \geqslant \lambda_a$. However, this is unreasonable. As Fig. 3 illustrates, for a surface without roughness elements ($\lambda = 0$), the transfer of momentum to the surface is determined by background turbulence. As roughness density increases, the transfer of momentum to the surface is affected by both background turbulence and wakes associated with roughness elements. As a result, the transfer of momentum is enhanced. As roughness density increases to $\lambda > \lambda_a$, mutual sheltering among the roughness elements becomes more important and thereby reduces the pressure drag on individual roughness elements, hence the transfer of momentum from the atmosphere to the surface. If the surface is fully covered by roughness elements, the background turbulence

is again the dominant mechanism for momentum transfer. The general trend of u_*/U_r variation with λ therefore must be as follows: it increases with λ if λ is small, reaches a maximum at λ_a and then decreases with λ if λ exceeds λ_a.

For small λ, Eq. (9) is based on sound physics. We therefore retain the functional form of this relationship, but replace λ with λ_e, i.e.

$$\frac{U_r}{u_*} = (C_S + \lambda_e C_R)^{-1/2} \exp\left(\frac{c\lambda_e}{2}\frac{U_r}{u_*}\right). \tag{10}$$

Eq. (10) is almost identical to Eq. (9) and fits well to experimental data for small λ and at the same time, it behaves rationally for large λ. The variations of u_*/U_r with λ estimated using different expressions are shown in Fig. 4. Both Eqs. (9) and (10) fit well to the observations of Raupach et al. (1980) and O'Loughlin (1965) for small λ. In general, Eq. (10) suggests that u_*/U_r first increases with λ, reaches a maximum at about $\lambda = 0.2$ and then decreases with λ.

2.1. Drag partition

The functional form for the ratio between the pressure drag and the total drag follows Raupach (1992), without repeating the details, but in terms of λ_e:

$$r_{tp} = \frac{\tau_{tp}}{\tau} = \frac{\beta\lambda_e}{1+\beta\lambda_e}. \tag{11}$$

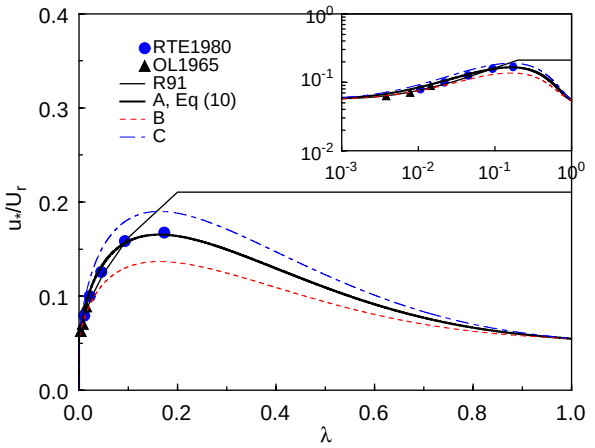

Fig. 4. Variation of u_*/U_r with λ, calculated using Eq. (9) with $c = 0.37$, $\beta = 100$ and $\lambda_a = 0.2$. Three calculations are done using Eq. (10) with $a = 6$, $n = 0.1$ and β for case A, $\beta = 150$ for case B and $\beta = 200$ for case C. The data of Raupach et al. (1980), RTE1980, and O'Loughlin (1965), OL1965, are used for comparison.

For the other two drag components, we have

$$\frac{\tau_{ts}}{\tau} + \frac{\tau_{tb}}{\tau} = 1 - \frac{\beta\lambda_e}{1+\beta\lambda_e}. \tag{12}$$

As τ_{ts} must decrease rapidly with increasing roughness density, we propose

$$r_{ts} = \frac{\tau_{ts}}{\tau} = \left(1 - \frac{\beta\lambda_e}{1+\beta\lambda_e}\right)\exp(-b_s\eta), \tag{13}$$

$$r_{tb} = \frac{\tau_{tb}}{\tau} = \left(1 - \frac{\beta\lambda_e}{1+\beta\lambda_e}\right)[1 - \exp(-b_s\eta)], \tag{14}$$

where b_s is an empirical parameter.

A comparison of r_{tp} estimated using Eq. (11) with the data of Marshall (1971) is shown in Fig. 5a. The estimates agree well with the measurements for small λ. The observations show that r_{tp} has a some scatter for different types of roughness elements. For Eq. (11) to fit well to the data, it is necessary to vary β in the range between 100 and 200. If $\beta = 150$ is selected, the proposed drag partition is almost identical to the Raupach (1992) scheme for $\lambda \leqslant 0.1$. In Eq. (13), we have set $b_s = 5$. The reason for this choice is to ensures that for small λ (recall Eq. (6)), r_{ts} is almost identical to that of Raupach (1992), (namely, τ_{ts}/τ in Eq. (3)) and for large λ, r_{ts} decays sufficiently fast to zero (Fig. 5b).

Our scheme requires τ_{tp}/τ to decrease to zero as $\lambda \to \lambda_{max}$, accompanied by τ_{tb}/τ increasing to one (Fig. 5c). We are not aware of observed data for verifying these scheme estimates. We have therefore conducted large-eddy simulations of flow over regular arrays of roughness elements with various roughness densities and then estimated drag partitions from the numerical results. The procedure of the large-eddy simulation is described in the Appendix. As shown in Fig. 5c, the numerical results support our drag partition scheme.

3. Roughness length and zero-displacement height

In a neutral surface layer, the profile of mean wind is approximately logarithmic

$$u(z) = \frac{u_*}{\kappa}\ln\left(\frac{z-d}{z_0}\right), \tag{15}$$

where $u(z)$ is the mean wind speed at height z and κ is the von Karman constant. For studying scalar transfer over rough surfaces, simple expressions for determining z_0 and d, in particular their dependencies on λ and η, are desirable. As outlined in Section 3.1, a number of studies on the subject have been

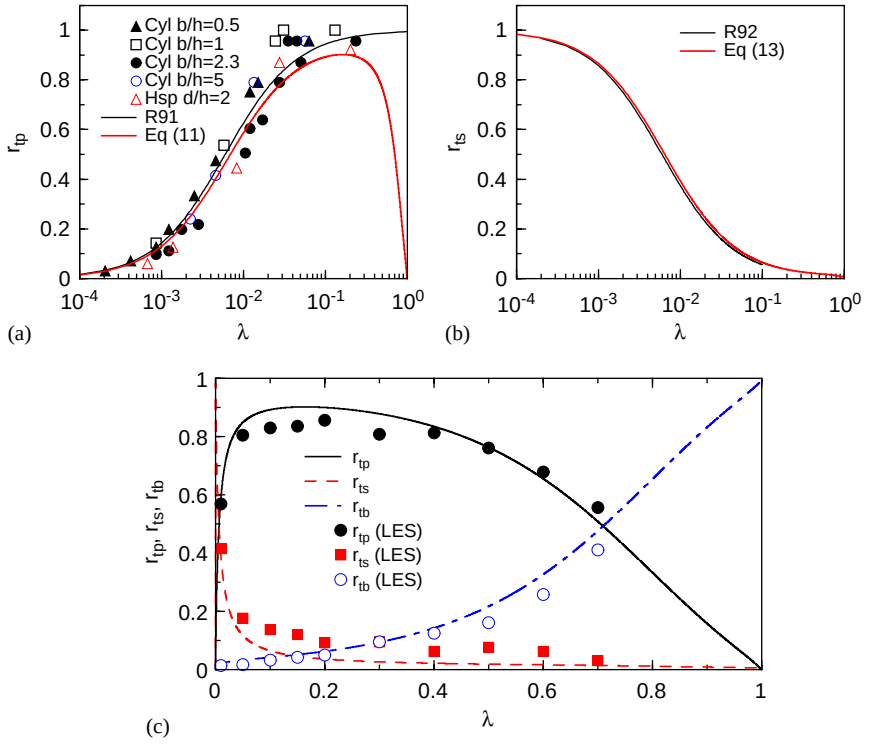

Fig. 5. (a) Comparison of pressure drag (in terms of $\sqrt{\tau_{tp}/\tau}$) calculated using Eq. (11) with the data of Marshall (1971); (b) comparison of surface drag calculated using Eq. (13); and (c) dependence of drag partition on λ calculated using Eqs. (11), (13) and (14). The values of a, n and β are respectively set to 6, 0.1 and 150. The symbols represent the results from large-eddy simulation. In (a) and (b), the estimates of r_{tp} and r_{ts} using the Raupach (1992) model are also shown.

carried out. In this study, we derive the estimates of z_0 and d based on drag partition. Our study offers an alternative method for determining z_0 and d over rough surfaces. The estimated z_0 and d are compared with observed data, and this comparison serves as an indirect validation of our drag partition scheme.

3.1. Existing methods for estimating z_0

Empirical relationships between z_0 and λ have been proposed in the literature. Lettau (1969) suggested

$$\frac{z_0}{h} = 0.5\lambda. \tag{16}$$

Counihan (1971) measured z_0 from velocity profiles in a wind-tunnel experiment over regular arrays of cubic elements and found that

$$\frac{z_0}{h} = 1.8\lambda - 0.08 \quad 0.06 < \lambda < 0.15. \tag{17}$$

Based on field and wind tunnel experiments, Theurer (1973) suggested that

$$\frac{z_0}{h} = 1.6\lambda(1 - 1.67\eta) \quad \lambda < 0.25. \tag{18}$$

Bottema (1996) suggested that

$$\frac{z_0}{h} = \frac{z_r - d}{h} \exp\left(-\frac{\kappa}{\sqrt{0.5\lambda C_D}}\right) \tag{19}$$

and to estimate d from the circulation zone volume. The method proposed by Bottema (1996) for the determination of C_D is rather complicated. Macdonald et al. (1998) proposed the following relationship:

$$\frac{z_0}{h} = \left(1 - \frac{d}{h}\right) \exp\left\{-\left[0.5\alpha \frac{C_D}{\kappa^2}\left(1 - \frac{d}{h}\right)\lambda_f\right]^{-0.5}\right\}, \tag{20}$$

where the displacement height d, is given by

$$\frac{d}{h} = 1 + A^{-\lambda}(\lambda - 1). \tag{21}$$

The best fit to wind-tunnel data is achieved by setting $A = 4.43$ for staggered arrays and $A = 3.59$ for the square arrays of roughness elements. On average, A is approximately 4. The value of $\alpha = 0.55$ in Eq. (20) is calibrated against experimental data.

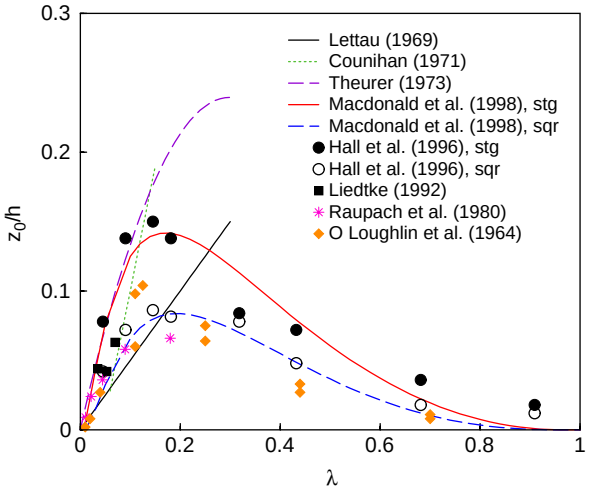

Fig. 6. Variation of z_0/h with λ estimated using various empirical relationships. Symbols represent the observations of O'Loughlin and MacDonald (1964), Raupach et al. (1980), Liedtke (1992) and Hall et al. (1996).

Fig. 6 shows the variation of z_0/h with λ for cubic obstacles, with the symbols representing the observations of O'Loughlin and MacDonald (1964), Raupach et al. (1980), Liedtke (1992) and Hall et al. (1996). There is a reasonable agreement among the estimates of the various empirical relationships and measurements for $\lambda<0.15$. Eqs. (16)–(18) predict a monotonic increase of z_0/h with λ and overestimate z_0/h when λ exceeds about 0.2. Eq. (20) fits well to the observations and reproduces the trend that z_0/h drops off after peaking at about $\lambda = 0.15$. Eq. (20) is derived by assuming wind profile is logarithmic with a displacement height d, there is negligible wake interference between the surface obstacles and the mean wind profile approaching each obstacle is logarithmic.

3.2. Zero-plane displacement

Thom (1971) suggested that d is the mean height of momentum absorption by the rough surface or the centroid of the drag force profile. This suggestion is supported by Jackson (1981) and Raupach (1992). This implies that d can be expressed as

$$d = (\tau_{ts}d_{ts} + \tau_{tp}d_{tp} + \tau_{tb}d_{tb})/\tau, \tag{22}$$

where d_{ts}, d_{tp} and d_{tb} are respectively the centroid of τ_{ts}, τ_{tp} and τ_{tb}. Since $d_{ts} = 0$ and $d_{tb} = h$, we have

$$\frac{d}{h} = \frac{\tau_{tp}}{\tau}\frac{d_{tp}}{h} + \frac{\tau_{tb}}{\tau}. \tag{23}$$

This relationship has the correct limiting behavior for any sensible choice of d_{tp}/h, i.e., if the surface is free of roughness elements, then $d/h = 0$; if the surface is full of roughness elements, then $d/h = 1$. Raupach (1992) argued that

$$\frac{d_{tp}}{h} = 1 - \frac{c_d}{\sigma_c}\frac{u_*}{U_h}, \tag{24}$$

where c_d is an O(1) constant and $\sigma_c = h/w_c$ with w_c being a typical streamwise inter-element distance. This relationship is difficult to use if $\sigma_c \to 0$. It is more robust to assume simply that

$$\frac{d_{tp}}{h} = \eta^k. \tag{25}$$

In Fig. 7, we compare d estimated by using Eq. (23) for several choices of k with that estimated by using Eq. (21) and the wind-tunnel data of Hall et al. (1996). The comparison shows that Eq. (23) agrees well with the wind-tunnel data by choosing $k \approx 0.5$. Tests using $k = 0.4$ and 0.6 are shown. As seen, d is not too sensitive to k.

3.3. Roughness length

The momentum flux and wind gradient relationship can be expressed as

$$\tau = \rho K\frac{\partial u}{\partial z},$$

where K is eddy viscosity. A friction velocity u_{*a} can be used to represent τ, i.e.,

$$u_{*a} = \sqrt{\rho^{-1}\tau}.$$

Both u_{*a} and K are functions of height

$$u_{*a} = g(z),$$
$$K = f(z)u_{*a}.$$

Assuming $u(d + z_0) = 0$, we have

$$u(z) = \int_{d+z_0}^{z}\frac{g(z)}{f(z)}\,\mathrm{d}z.$$

The logarithmic wind profile is the special case of $g(z) = c$ (i.e. u_*) and $f(z) = \kappa(z - d)$. For rough-surface atmospheric boundary layers, this logarithmic relationship is valid for $z > z_w$ where z_w is several times the height of the roughness elements. At $z = z_w$, we expect that

$$u(z_w) = \frac{u_*}{\kappa}\ln\left(\frac{z_w - d}{z_0}\right). \tag{26}$$

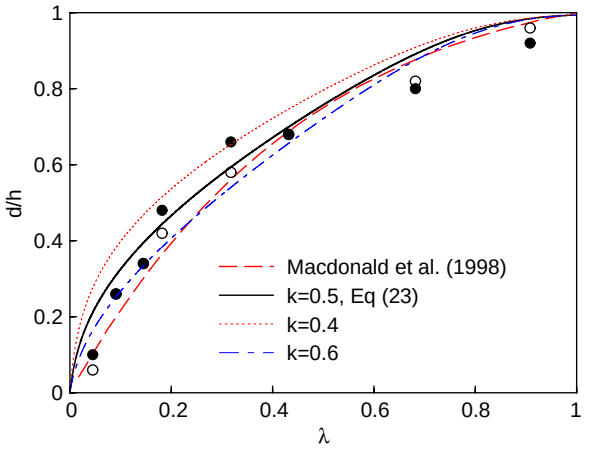

Fig. 7. Comparison of d estimated using Eq. (23) for three choices of k with d estimated from Eq. (21) with $A = 4$ and wind-tunnel data of Hall et al. (1996).

To determine z_0, an estimate of $u(z_w)$ is required. The total drag τ can be partitioned into τ_{tp}, τ_{ts} and τ_{tb}, but τ_{tp} distinguishes from τ_{ts} and τ_{tb} in that it is related to the mean wind speed while the other two are related to wind shear. It is hence reasonable to argue that wind shear in the regime of $z < z_w$ determines $(\tau_{tb} + \tau_{ts})$.

Similar to Eq. (22), the centroid of $(\tau_{tb} + \tau_{ts})$ can be calculated by

$$d_a = \frac{\tau_{ts} d_{ts} + \tau_{tb} d_{tb}}{\tau_{ts} + \tau_{tb}} = \frac{\tau_{tb}}{\tau_{ts} + \tau_{tb}} h \tag{27}$$

as $d_{ts} = 0$ and $d_{tb} = h$. This implies that the collective effect of τ_{tb} and τ_{ts} absorbed respectively at d_{tb} and d_{ts} is equivalent to that of $(\tau_{ts} + \tau_{tb})$ absorbed at d_a. It is now convenient to introduce a shear-generated momentum flux τ_a which varies with height from $\tau_{ts} + \tau_{tb}$ at d_a to τ at z_w. The corresponding friction velocity u_{*a} varies linearly with height, from $u_{*a0} = \sqrt{(\tau_{ts} + \tau_{tb})/\rho}$ at d_a to u_* at z_w, i.e.,

$$u_{*a} = u_* \left[r + (1 - r) \frac{z - d_a}{z_w - d_a} \right], \tag{28}$$

where

$$r = \sqrt{1 - \tau_{tp}/\tau}. \tag{29}$$

The relationship between u_{*a} and the mean flow speed for the region $d_a + z_{0s} \leqslant z \leqslant z_w$ (z_{0s} is the roughness length of roughness element surface) is then reconstructed as

$$u_{*a}^2 = K \frac{\partial u}{\partial z},$$

with $K = \kappa u_{*a}(z - d_a)$. An integration of the above relationship leads to

$$u_w = \frac{r u_*}{\kappa} \ln\left(\frac{z_w - d_a}{z_{0s}} \right) + \frac{u_*(1 - r)(z_w - d_a - z_{0s})}{\kappa(z_w - d_a)}. \tag{30}$$

A comparison of Eqs. (30) and (26) suggests that z_0 can be expressed as

$$z_0 = (z_w - d) \left(\frac{z_{0s}}{z_w - d_a} \right)^r \exp(r - 1). \tag{31}$$

Existing observations indicate that z_w varies from case to case. According to Cheng and Castro (2002), when the wind profile is spatially averaged the logarithmic layer extends down to the roof level, suggesting that $z_w = h$. In studying boundary layers over vegetation canopies, Raupach (1992) argued that

$$z_w - d = c_w(h - d),$$

where c_w is about 4. In this study, we assume $z_w = c_w h$ with c_w being a constant between 1 and 4.

We use the wind-tunnel data of Hall et al. (1996) together with the several other wind-tunnel data sets to verify Eq. (31). The wind tunnel experiments of Hall et al. (1996) were conducted for square and staggered arrays of roughness elements. The roughness elements are cubes of 0.01 m in height (for cubic roughness elements, $\lambda = \eta$). Fig. 8 shows the comparison of z_0/h estimated using Eq. (31) and the

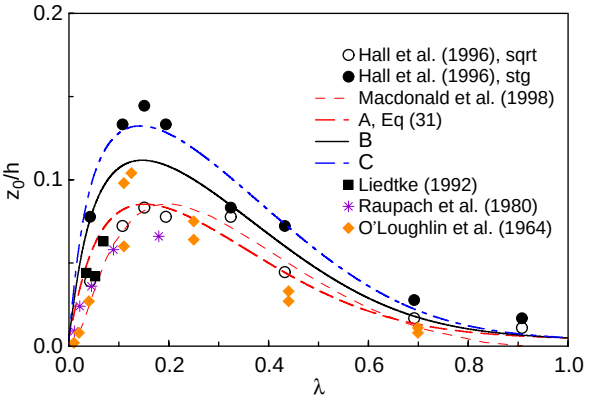

Fig. 8. Comparison of z_0/h estimated using Eq. (31) with the wind-tunnel data of Hall et al. (1996) for the square-array and staggered-array cases of cubic roughness elements of 0.1 m. For curve A, $\beta = 100$ and $z_w = 1.5h$ are used; for curve B $\beta = 150$ and $z_w = 1.5h$ are used; and for curve C, $\beta = 180$ and $z_w = 2h$ are used. Curve A fits well to the data for the square-array case and curve C fits well to the data of the staggered-array case. The observations of O'Loughlin and MacDonald (1964); Raupach et al. (1980) and Liedtke (1992) are also shown for comparison.

wind-tunnel observations. For the square-array case, $\beta = 100$ and $z_w = 1.5h$ are set and for the staggered-array case, $\beta = 180$ and $z_w = 2h$ are used. The qualitative behavior of z_0, as observed in the wind-tunnel experiments, is reproduced by the model, i.e., z_0 first increases with λ to a maximum at around $\lambda = 0.2$ and then decreases to z_{0s} as λ further increases. The wind-tunnel observations show that z_0 varies from case to case, e.g., z_0 for the staggered-array case is considerably larger than for the square-array case of roughness elements. We believe this is caused by the fact that the staggered-array case generates a deeper mixing layer and therefore, a larger z_w and β must be selected. Our study offers an alternative method for the calculation of z_0 and d to the method of Macdonald et al. (1998). By adjusting the empirical factors A and α in (20) and (21), the method of Macdonald et al. can quite well approximate z_0 and d for both cases square and staggered arrays.

4. Concluding remarks

We have presented a drag partition scheme for rough surfaces. We have argued that the scheme of Raupach (1992), which is valid for rough surface of small roughness density, can be extended to rough surface of large roughness density by introducing the effective frontal area index, λ_e. This index describes the mutual sheltering effect among the roughness elements. For small roughness density, λ_e approaches λ, while for large roughness density, λ_e approaches zero. We have proposed a workable expression for λ_e [Eq. (8)] which satisfy several constraints.

We have argued that the total drag can be partitioned into three components: a pressure drag, a surface drag and a skin drag. Simple expressions can be used for the calculation of these drag components. For small λ, the estimated pressure and surface drag are in good agreement with wind tunnel data. For large λ, we do not have observations for the verification of the scheme, but have carried out large-eddy simulation for comparison. The large-eddy simulation results support the drag partition scheme. Direct measurements of drag partition components, especially for cases of large λ, are nevertheless desirable for further validation of the scheme.

Based on drag partition, schemes for the calculation of zero-plane displacement height, d, and roughness length, z_0, have been proposed. This approach differs from those of Bottema (1996) and Macdonald et al. (1998). We have compared the estimates of d and z_0 with the wind-tunnel experiment data of Hall et al. (1996) and have found that our calculations are in good agreement with the data. The favorable comparison indirectly confirms the correctness of the drag partition scheme. The zero-plane displacement height is found to increase with λ, from 0 to h. It is also found that for small λ, z_0 increases with λ, reaching an maximum at around $\lambda = 0.2$ and then decreases with λ. This behavior of z_0 reflects the impacts of roughness distribution on the atmospheric boundary layer. At small λ, roughness elements exist as individuals and the sheltering effect is weak, the impact of the roughness elements is to increase momentum transfer. As λ becomes larger, mutual interference among roughness elements becomes larger, thereby decreasing the capacity of the surface to absorb momentum.

While the drag partition scheme should be applicable for rough surfaces with roughness elements of arbitrary aspect ratio, we have mainly used wind-tunnel data for solid cubic roughness elements for the validation. As Fig. 8 implies, quantities such as z_0/h may exhibit considerable differences for surfaces with different configurations and characteristics of roughness elements. For porous roughness elements and roughness elements with aspect ratio other than one, we expect that drag partition terms and the associated physical quantities, such as d and z_0, to be somewhat different from what has been presented in this study. However, these situations can be sufficiently well covered by choosing different β values in the drag partition scheme, as partially illustrated in Figs. 4 and 8. Wyatt and Nickling (1997) showed that for sparsely vegetated desert canopies, β is around 200 rather than 120 typically used for solid blocks.

In this study, we have derived expressions for d and z_0 as one application of the drag partition scheme, but the drag partition scheme is also useful to the study of scalar transfer in atmospheric boundary layers over rough surfaces (e.g. calculation of aerodynamic conductance). A scalar transfer scheme for urban boundary layers has been derived by Yang and Shao (2005) by taking advantage of the scheme presented in this paper.

Acknowledgements

The work described in this paper was fully supported by a grant from the Research Grants

Council of the Hong Kong Special Administrative Region, China (Project no. CityU 1212/01 P).

Appendix

For the calculation of r_{tp}, r_{ts} and r_{tb}, large-eddy simulations are performed using the Computational Fluid Dynamics code CFX (AEA Technology, Harwell). The Smagorisky subgrid closure is used for the simulation. The domain of simulations is $1\,m \times 1\,m \times 1\,m$. The surface is covered with regular arrays of roughness elements (cubes of 0.1 m in length). Unstructured mesh is used. Periodic boundary conditions are used in the direction of the mean flow. In doing so, the numerical experiment mimics the situation of flow over an infinitely long rough surface. The upper boundary is specified as a symmetry plane and a non-slip boundary condition is applied to the lower boundary. The initial wind speed is set to $1\,m\,s^{-1}$. The temperature is kept constant at 293 K; this also implies that the flow is neutrally stratified. The underlying surface and the surfaces of the roughness elements are assumed to be rough walls with roughness length $z_0 = 0.0005\,m$. A total of 10 experiments are carried out with λ varying from 0.01 to 0.7.

We denote the side surface of the roughness elements as $s1$, the top surface of the roughness elements as $s2$ and the ground surface as $s3$. The pressure drag is calculated as an integration of pressure, p, over $s1$

$$\tau_{tp} = \int\int_{s1} p\,dx\,dz/S.$$

The skin drag τ_{tb} is calculated as an integration of wall shear over $s2$

$$\tau_{tb} = \int\int_{s2} \tau_{wall}\,dx\,dy/S$$

and the surface drag is obtained by integration of wall shear over $s3$,

$$\tau_{ts} = \int\int_{s3} \tau_{wall}\,dx\,dy/S.$$

References

Arya, S.P.S., 1975. A drag partition theory for determining the large-scale roughness parameter and wind stress on the Arctic Pack Ice. Journal of Geophysical Research 80, 3447–3454.

Bottema, M., 1996. Roughness parameters over regular rough surfaces: experimental requirements and model validation. Journal of Wind Engineering and Industrial Aerodynamics 64, 249–265.

Cheng, H., Castro, I.P., 2002. Near wall flow over an unban-like roughness. Boundary-Layer Meteorology 104, 229–259.

Counihan, J., 1971. Wind tunnel determination of the roughness length as a function of the fetch and the roughness density of three-dimensional roughness elements. Atmospheric Environment 5, 637–642.

Crawley, D.M., Nickling, W.G., 2003. Drag partition for regularly-arrayed rough surfaces. Boundary-Layer Meteorology 107, 445–468.

Gillies, J.A., Lancaster, N., Nickling, W.G., Crawley, D.M., 2000. Field determination of drag forces and shear stress partitioning effects for a desert shrub (Sarcobatus vermiculatus, Greasewood). Journal of Geophysical Research 105, 24,871–24,880.

Hall, D.J., Macdonald, R., Walker, S., Spanton, A.M., 1996. Measurements of dispersion within simulated urban arrays—a small scale wind tunnel study. BRE Client Report CR 178/96, Building Research Establishment, Garston Watford.

Harman, I.N., Barlow, J.F., Belcher, S.E., 2004. Scalar fluxes from urban street canyons. Part II: modelling study. Boundary-Layer Meteorology 113, 387–410.

Jackson, P.S., 1981. On the displacement height in the logarithmic velocity profile. Journal of Fluid Mechanics 111, 15–25.

Lettau, H., 1969. Note on aerodynamic roughness parameter estimation on the basis of roughness element description. Journal of Applied Meteorology 8, 828–832.

Liedtke, J., 1992. An experimental investigation into the dispersion behaviour in neutral and unstable zero pressure gradient boundary layers with different roughnesses. (In German: Experimentelle Untersuchung des Ausbreitungsverhaltens eines gasformigen Stoffes in neutral und instabil geschichteten turbulenten Gleichdruckgrenzschichten bei unterschiedlicher Bodenrauhigkeir.) Ph.D. Thesis, Universität der Bundeswehr, München, FRG.

Macdonald, R.W., Griffiths, R.F., Hall, D.J., 1998. An improved method for the estimation of surface roughness of obstacle arrays. Atmospheric Environment 32, 1857–1864.

Marshall, J.K., 1971. Drag measurements in roughness arrays of varying density and distribution. Agricultural Meteorology 8, 269–292.

O'Loughlin, E.M., 1965. Resistance to flow over boundaries with small roughness concentrations. Ph.D. Dissertation, University of Iowa.

O'Loughlin, E.M., MacDonald, E.G., 1964. Some roughness-concentration effects on boundary resistance. La Houille Blanche 7, 773–782.

Raupach, M.R., 1992. Drag and drag partition on rough surfaces. Boundary-Layer Meteorology 60, 374–396.

Raupach, M.R., Thom, A.S., Edwards, I., 1980. A wind tunnel study of turbulent flow close to regularly arrayed rough surfaces. Boundary-Layer Meteorology 18, 373–397.

Raupach, M.R., Gillette, D.A., Leys, J.F., 1993. The effect of roughness elements on wind erosion thresholds. Journal of Geophysical Research 98, 3023–3029.

Schlichting, H., 1936. A wind tunnel study of turbulent flow close to regularly arrayed rough surfaces. Ing.-Arch. NACA Technical Memorandom 823, vol. 7, pp. 1–34.

Theurer, W., 1973. Dispersion of ground-level emissions in complex built-up areas. Ph.D. Thesis, University of Karlsruhe (in German).

Thom, A.S., 1971. Momentum absorption by vegetation. Quarterly Journal of Royal Meteorology Society 97, 414–428.

Wolfe, S.A., Nickling, W.G., 1996. Shear stress partitioning in sparsely vegetated desert canopies. Earth Surface Processes and Landforms 21, 607–619.

Wooding, R.A., Bradley, E.F., Marshall, J.K., 1973. Drag due to regular arrays of roughness elements of varying geometry. Boundary-Layer Meteorology 5, 285–308.

Wyatt, V.E., Nickling, W.G., 1997. Drag and shear stress partitioning in sparse desert creosote communities. Canadian Journal of Earth Sciences 34, 1486–1498.

Yang, Y., Shao, Y., 2005. A scheme for scalar exchange in urban boundary layers. Boundary-Layer Meteorology, accepted.